

We are IntechOpen, the world's leading publisher of Open Access books Built by scientists, for scientists

6,900

Open access books available

186,000

International authors and editors

200M

Downloads

Our authors are among the

154

Countries delivered to

TOP 1%

most cited scientists

12.2%

Contributors from top 500 universities



WEB OF SCIENCE™

Selection of our books indexed in the Book Citation Index
in Web of Science™ Core Collection (BKCI)

Interested in publishing with us?
Contact book.department@intechopen.com

Numbers displayed above are based on latest data collected.
For more information visit www.intechopen.com



Erosion Behavior of Plasma Sprayed Alumina and Calcia-Stabilized Zirconia Coatings on Cast Iron Substrate

N. Krishnamurthy¹, M.S. Murali², B. Venkataraman³ and P.G. Mukunda⁴

¹Mechanical Engineering Department, K.S. Institute of Technology, Bangalore,

²Auden Technology and Management Academy, Bangalore,

³Surface Engineering Group, Defence Metallurgical Research Laboratory,
Kanchanbagh, Hyderabad,

⁴Mechanical Engineering Department, Nitte Meenakshi Institute of Technology,
Bangalore,
India

1. Introduction

In plasma arc spraying process also known as plasma spraying process, the thermal energy of an electric arc (40 kW or 80kW) together with a plasma forming gas, which would be either nitrogen or argon, are utilized in melting and propelling of the deposit material at high velocities (600 mS^{-1}) onto a substrate. This process is capable of generating very high temperature, exceeding $16,000 \text{ }^\circ\text{C}$, which can be gainfully employed in the deposition of materials with high melting points. The deposited material is generally in a powder form and requires a carrier gas to feed it into the combustion chamber. The process enables discharging high bond strengths of the coatings due to the very high propulsion velocities of the impinging particles.

In a DC plasma arc process, gas heating is enough to generate core plasma temperatures exceeding $20000 \text{ }^\circ\text{C}$ depending upon the properties of gas and its electrical break down characteristics. Enthalpy of the gas is an indicator of its heating potential while it is getting translated to plasma state.

1.1 Special features of plasma spraying technique

The following are some of the unique features of the plasma spraying process.

- The technique can be used to deposit a wide range of ceramics and metals and their combinations as well.
- It is possible to deposit alloys and mixed ceramics with components of widely differing vapor pressures without significant changes in composition.
- Homogenous coatings can be formed for any composition while maintaining uniformity in their thickness.

- Fine microstructures with equiaxed grains and without any type of columnar defects are the characteristics of this process.
- High deposition rates are possible without huge investments on capital equipment.
- The process can be carried out virtually in any environment such as air, encoded inert low and high-pressure environments, or underwater.

1.2 Erosion wear

Erosive wear of the solid bodies is caused by the action of sliding or impact of solids, liquids, gases or a combination of these [1]. Erosion can be divided into three basic types: Solid particle erosion, liquid impact erosion and cavitations erosion. Cavitation erosion is the loss of material due to the repeated formation and collapse of bubbles in a liquid. Liquid impact erosion is the damage caused by water droplets. Solid particle erosion is a wear process where they strike against surfaces and promote material loss. It is also caused by the impact of hard particles carried by a fluid stream onto a material surface.

Solid particle erosion is an important material degradation mechanism encountered in a number of engineering systems such as thermal power plants, aircraft gas turbine engines, IC engines, pneumatic bulk transport systems, coal liquefaction/gasification plants and ore or coal slurry pipe lines. At the same time, the erosion process has been used to advantage in number of situations like sand blasting of castings, shot peening of rotating components, cutting of hard and brittle materials by abrasive jets and rock drilling [2, 3].

Manifestations of solid particle erosion in service usually include thinning of components, a macroscopic scooping appearance following the gas/particle flow field, surface roughening and lack of the directional grooving characteristic of abrasion and in some the formation of ripple patterns on metals. Solid particle erosion can occur in a gaseous or liquid medium containing solid particles. In both the cases, particles can be accelerated or decelerated and their directions of motion can be changed by the fluid [4].

Power station boiler-walls and other utility parts of coal-fired plants are subjected to frequent degradation by erosion-corrosion problems relevant to the reliability and economics of these installations. The environment inside the furnaces is characterized by high-temperature conditions together with aggressive atmospheres, leading to corrosive deposits adhering into the walls and to erosion processes caused by the ash particles [5].

In erosion, several forces of different origins may act on a particle in contact with a solid surface. Neighboring particles may exert contact forces and a flowing fluid, if present, will cause the drag. On some situations, gravity may also be important. However, the dominant force on an erosive particle, which is mainly responsible for decelerating it from its initial impact velocity, is usually the contact force exerted by the surface. Erosion of metals usually involves plastic flow, whereas more brittle materials may wear predominantly either by flow or by fracture depending on the impact conditions [6].

Solid particle erosion behavior of most of the materials can be categorized as being either brittle or ductile in nature [7]. The major differentiating characteristic of the two types of mechanism is the dependence of erosion rate on impact angle i.e. the angle between the moving erodent particle and the material surface [8]. There is general agreement that maximum erosion occurs at a low angle (about 30°) for ductile material and at 90° for brittle

material. Figure shows the schematic of the expected variation in erosion behavior with impact angles

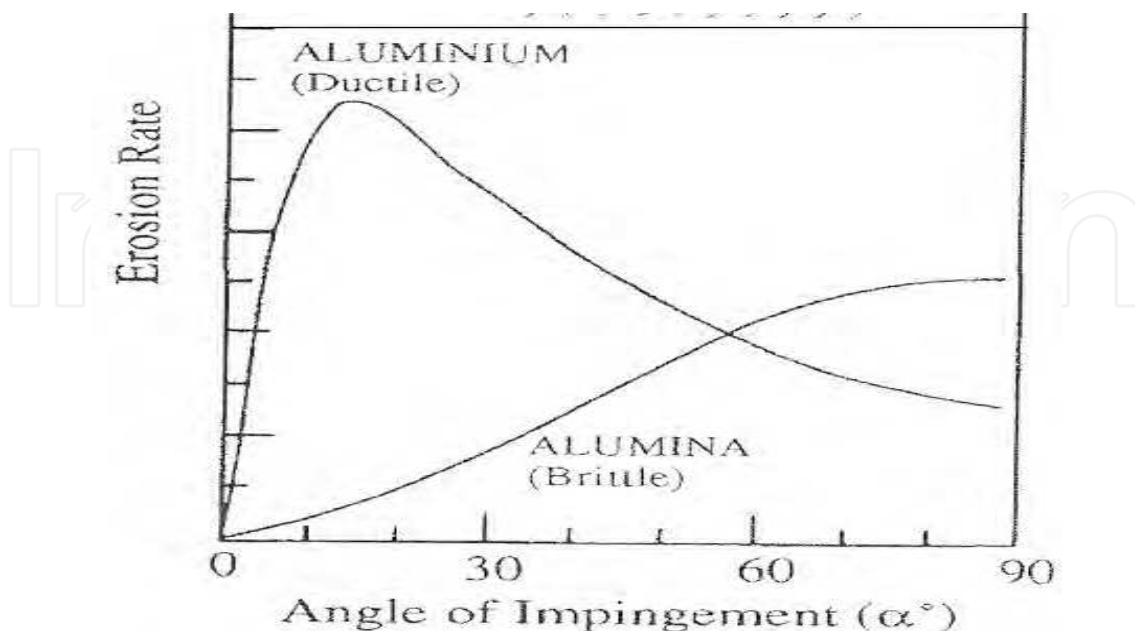


Figure Expected Variation of Erosion Rate with Particle Impact Angle (Ref. 8)

Most applications involve low impact angles at which erosion resistance of ceramics happens to be significant. It should also be noted, that the microstructure of plasma sprayed coatings often differs significantly from that of corresponding bulk material. The structure of plasma sprayed coatings consists of many overlapped lenticular splats which conform more or less either to the morphology of the underlying substrate or to that of previous splats. Although plasma sprayed coatings are anisotropic, their erosion rates tend to exhibit the same dependence on impact angle similar to that of the bulk material of ceramics [9]. On the other both Kingswell [10] and Zhang [11] have noted that the erosion mechanism in plasma sprayed alumina coating is different from those in bulk sintered alumina. Erosion of bulk ceramics generally occurs by a number of fracture mechanisms [12, 13]. During particle impact upon a ceramic surface, median and radial cracks develop at the impact site [14]. Upon rebounding of the particles i.e. unloading of the impact site, lateral cracks develop parallel to the surface and finally follows a curved path before propagating towards the surface, leading to chipping and loss of material. Erosion in plasma sprayed ceramics has been attributed to the failure of the individual splat boundaries.

2. Experimental details

2.1 Plasma spraying and characterization techniques

The surfaces of the substrate materials which are to be plasma coated were examined for dimensional accuracy and surface finish before being degreased in a vapour bath (70- 80°C) of tetra chloro ethylene. The surfaces were then grit blasted by Al_2O_3 (-18+24 mesh) at a pressure of 455 kPa. Plasma spraying process was carried out with the help of proprietary Sulzer Metco Equipment. The composition of cast iron substrate and coating materials is given in Table 1.

Substrate material			
Cast Iron			
C-3.54, Si-2.21, Mn-0.67, Cr-0.025, Cu-0.013, P-0.056, S-0.031, Fe-balance			
Coating material			
Metco105SFP (TC1)	Metco 210NS (TC2)	Metco 452 (BC1)	Metco 410NS (BC2)
99.5 Al ₂ O ₃	ZrO ₂ 5CaO	Fe 38Ni10Al	Al ₂ O ₃ 30(Ni 20Al)

TC1-Top Coat 1, TC2-Top Coat 2, BC1-Bond Coat 1, BC2-Bond Coat 2

Table 1. Chemical composition of substrate and coating materials

The schematic diagrams of coating layers on cast iron substrate are shown in Fig. 1. The spray parameters for different materials are shown in Table 2.

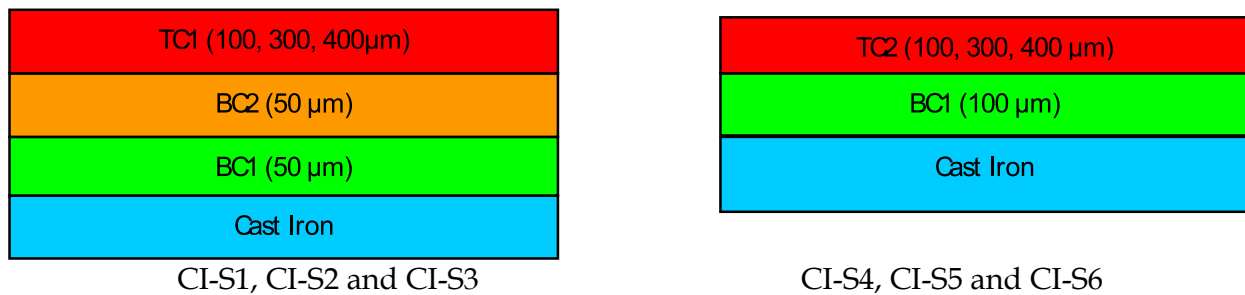


Fig. 1. Schematic diagrams of coating layers with cast iron substrate (number in the bracket indicates the required thickness of each layer)

Materials	Primary gas (Argon) pressure kPa	Secondary gas(H ₂) Pressure kPa	Carrier gas (Argon) Flow lpm	Current A	Voltage V	Spray distance mm	Feed rate kg/hr
TC1	700	520	60	600	65	64-125	2.7
TC2	345	345	37	500	75	50-100	5.4
BC1	700	340	37	500	65	100-175	4.1
BC2	700	340	37	500	65	100-175	4.1

Table 2. Plasma spray parameters

Surface texture of the coated samples was examined, employing Mahr Perthometer. The coated plate of 100x100 sq. mm area was selected and it was divided into small segments of 10 x 10 sq. mm. The tracing length was about 5.6 mm for each of the selected segment. Typical parameters describing the surface quality such as Arithmetical Mean Deviation or Average Roughness (Ra), Mean Roughness Depth (Rz), Maximum Roughness Depth (Rmax), Core Roughness Depth (Rk), Reduced Peak Height (Rpk), Distance between the Highest Profile Peak and the Reference Line (Rp), Root Mean Square Deviation (Rq) were recorded on each of the segments subjected to the analysis.

Microstructure analysis and surface morphology studies were carried out on a JOEL-JAPAN JSM-840A Scanning Electron Microscope. Area percentage measurements were done using a Leitz microscope fitted with a Biovis image Analyzer on the polished section of the coating. Care was taken to minimize the pull out of bond coat and top coat particles during polishing of the coated samples. The mounted samples were polished using emery papers of 240, 300, 400, 600 grit sizes and subsequently on 1/0, 2/0, 3/0 and 4/0 grades, successively. Fine polishing was done to obtain a mirror finish using 0.5 μm diamond impregnated cloth. The polished sample was cleaned with acetone before mounting on an optical microscope interfaced to a digital image capture and analysis system. The magnification was chosen such that the coating microstructure image covers the screen and allows the resolution of the voids that contributes significantly to the total porosity area percentage. The process of selecting the appropriate range of grey values was done to ensure that only voids were sampled. About ten separate fields of view were selected to ensure consistency in the analysis.

XRD analysis of the coated test samples were carried out on a Philips X-Ray Diffractometer (Model: PW 1840) using Cu-K α radiation over a 2θ range of 20 to 100 $^\circ$. The scanning speed was taken as 2 $^\circ$ per min.

For Adhesion test cast iron cylindrical substrates were prepared according to ASTM C633-79 standards. The circular face of the test sample was coated according to the procedure explained in first paragraph of this section. One more sample with the same geometry but without coating was then joined to this coated surface employing an adhesive, Epoxy Polymer 15 (EP 15) with the application of the contact pressure varying from 2-3bar. The sample was then heated to 170 $^\circ\text{C}$ and maintained at this temperature for more than 60 minutes, before cooling it to room temperature. The specimens thus prepared were tested in a UTM of 60 tones capacity. The maximum load, maximum tensile strength and the stress strain diagram for the specimen were displayed by the computer connected to UTM. On each sample, five tests were conducted.

The microhardness of the test samples was determined using Leica Vickers Microhardness Tester (Model: VHMT Auto) as per ASTM E384 [15] standards. The test parameters are; 300 g load, 25 $\mu\text{g S}^{-1}$ loading rate, 15 seconds dwell time with a Vickers Pyramid indenter. The measurement of hardness was done along the total thickness of the coating including substrate. An average of ten measurements taken at different locations on the transverse section of the coating was reported.

2.2 Solid particle erosion test

Erosion tests on coated and uncoated test samples were carried out according to ASTM G76-02 [16] standards. The test parameters are shown in Table 3. The sample was first cleaned in acetone using an ultrasonic cleaner, dried and then weighed using an electronic balance having a resolution of 0.01 mg. The sample was then fixed to the sample holder of the erosion rig and eroded with silica sand at the predetermined particle feed rate, impact velocity and impact angle for a period of about 5 min. The sample was then removed, cleaned in acetone and dried and weighed to determine the weight loss. This weight loss normalized by the mass of the silica particles causing it (i.e. testing time x particle feed rate) is then computed as the dimensionless incremental erosion rate. The above procedure was repeated till the incremental erosion rate attained a constant value independent of the mass of the erodent particles or, equivalently, of testing time. This constant value of the

incremental erosion rate is defined as the steady-state erosion rate. On each coating system, three tests were conducted. The test parameters are given in Table 3.

Erodent Material	Silica Sand (Angular)
Erodent Size (μm)	150-300
Particle Velocity (m/s)	40
Erodent Feed Rate (g/min)	4.3
Impact Angle ($^\circ$)	15, 45 and 90
Test Temperature	Room Temperature
Test Time (min)	5 minutes Cycles
Sample Size (mm)	30 x 30 x 5
Nozzle Diameter (mm)	4.5
Stand-off Distance (mm)	10

Table 3. Erosion Test Parameters

3. Results and discussion

3.1 Surface texture of coatings

Average roughness of different coatings is indicated in Table 4.

It is evident that the average roughness values of alumina coatings cast iron substrates vary between 3.5 and 5.5 μm and it is between 4.5 and 7.2 μm in case of $\text{ZrO}_2\text{5CaO}$ coatings. Top coat of test samples such as CI-S4, CI-S5, CI-S6 possess mounds of molten and unmolten particles contribute to the increase in roughness. Flowability of $\text{ZrO}_2\text{5CaO}$ is less compared to alumina and this contributes to the formation of mounds and affects the quality of the surface texture of the coating. Increase in porosity as well as the coating thickness enhances the roughness of top coat. Coating roughness also increases with enhanced coating thickness. Similar observations regarding to the effect of coating thickness on roughness were reported by O. Sarikaya [17].

Fig.2 shows the roughness profiles of few coating systems (CI-S2 and CI-S6) with average roughness (R_a) as the main parameter.

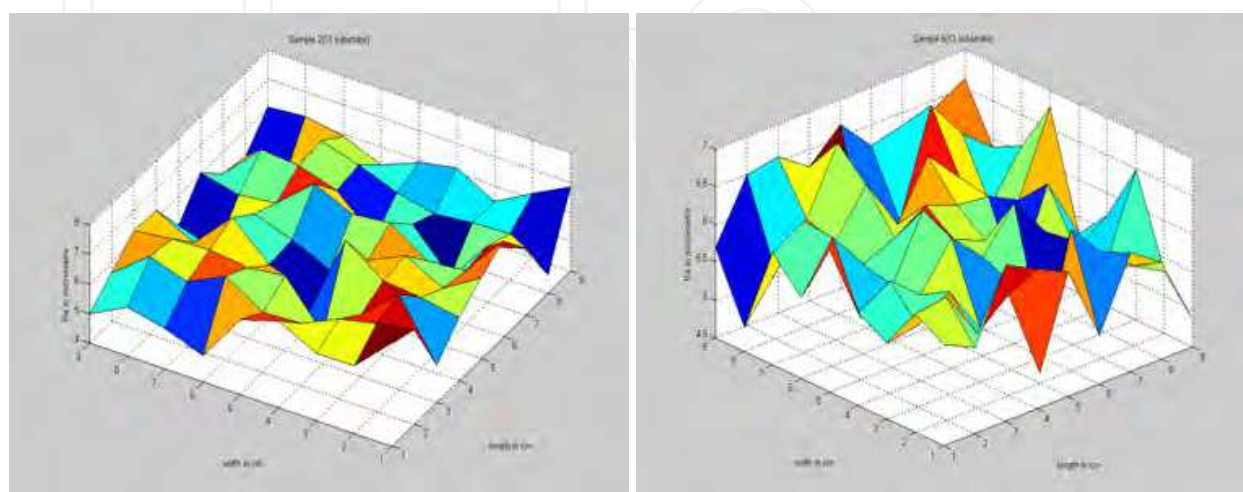
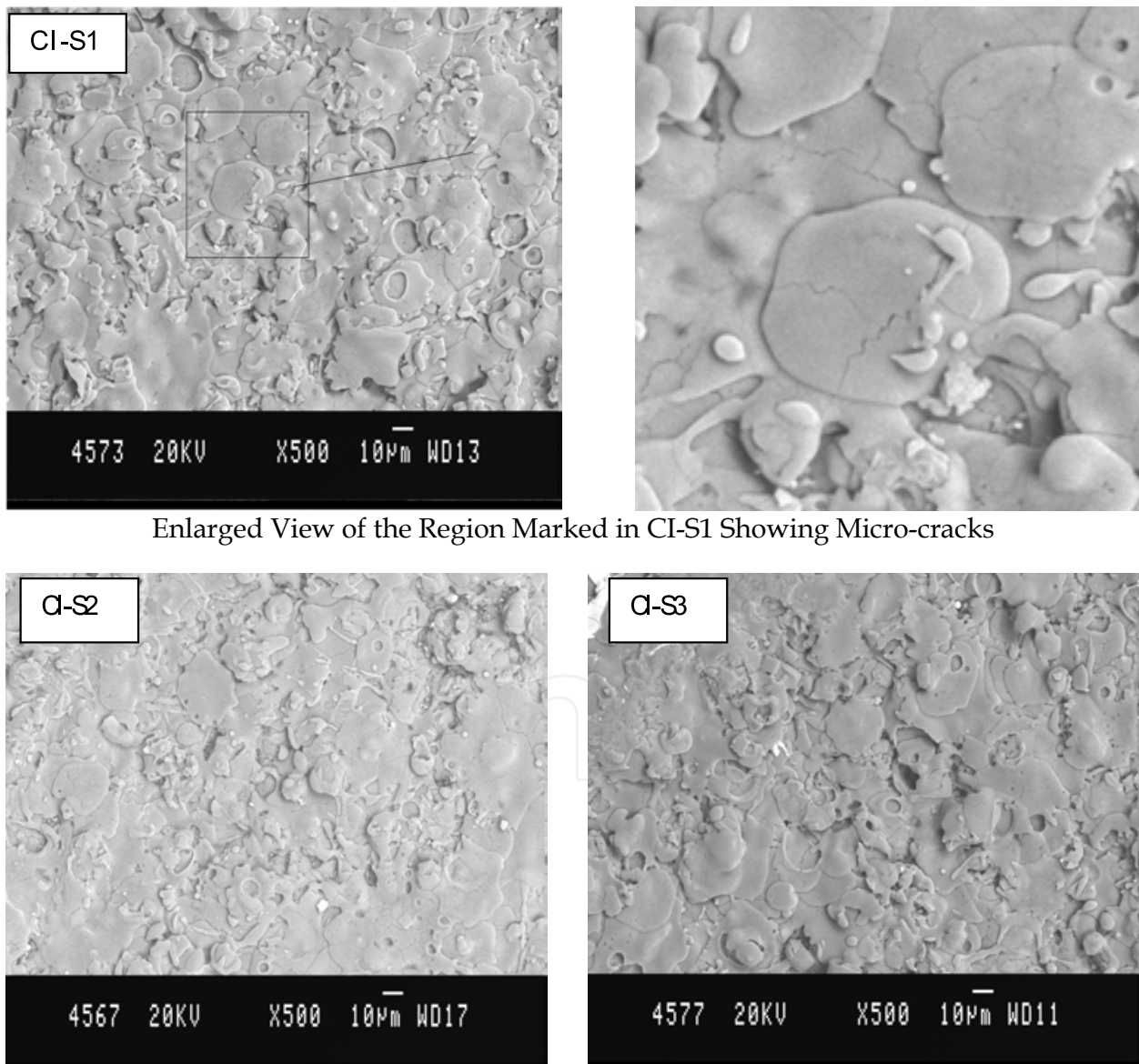


Fig. 2. Roughness profiles of coating systems

3.2 Morphology of coatings

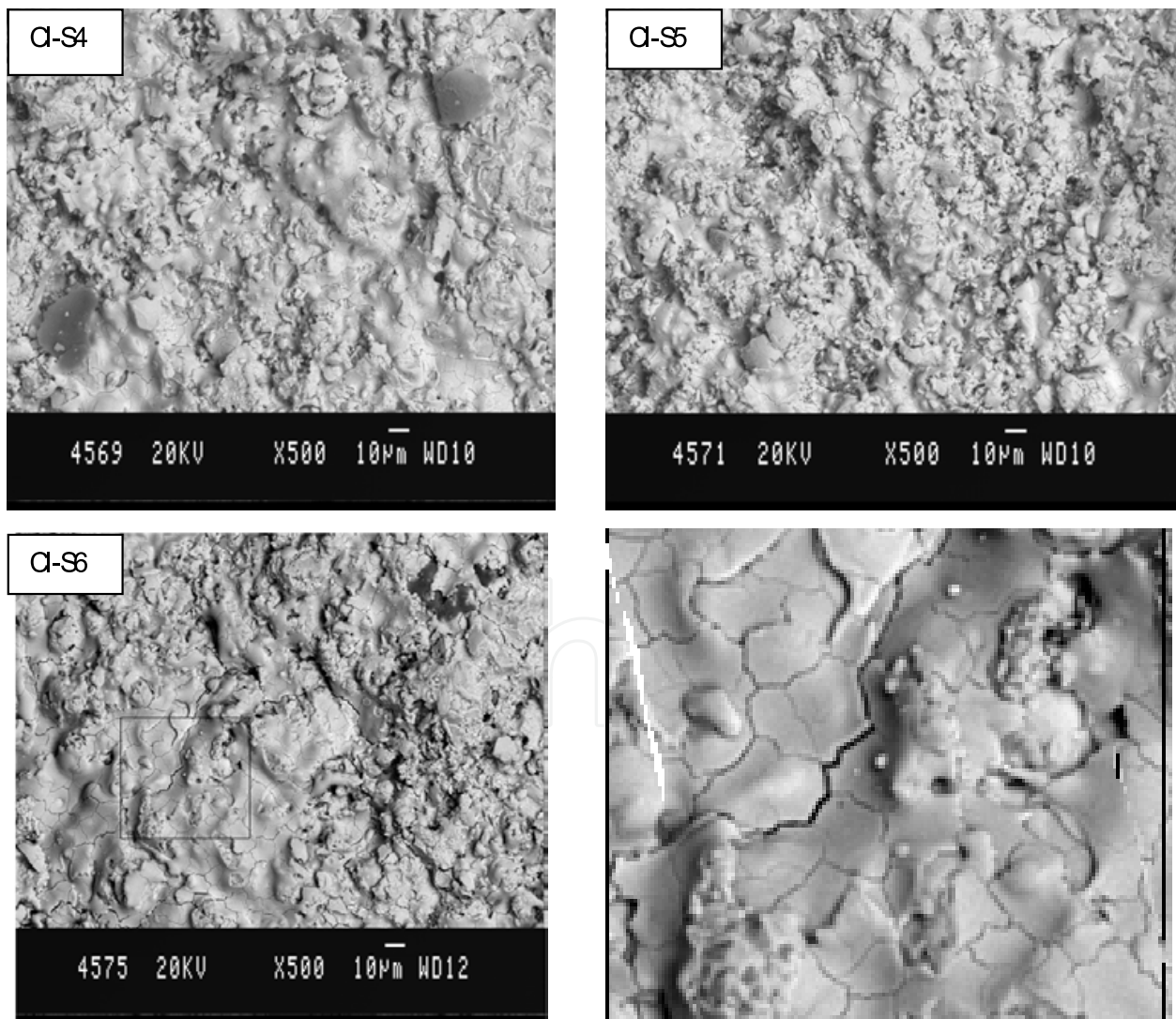
Al_2O_3 coated test samples viz., CI-S1, CI-S2, CI-S3 are characterized by their disc shaped grains (Fig.3). These grains are found to be the flattened solidified droplets of the coating material. The molten particles are found to be distributed more or less evenly producing a smooth coating surface. Enlarged view of marked region of CI-S1 sample (Fig.3) indicates a network of microcracks. Cracks are also observed on the surface of flattened droplets. This may be possibly due to the presence of residual stresses introduced by thermal shocks resulted during the spraying process. Changing the thickness of top coat appears to have no significance on the microstructure as in the case with test samples CI-S2, CI-S3 (Fig.3).



Enlarged View of the Region Marked in CI-S1 Showing Micro-cracks

Fig. 3. Topology of Al_2O_3 Coatings Cast Iron

ZrO₂5CaO coated test samples such as CI-S4, CI-S5, CI-S6 exhibit a dense undulated structure (Fig.4). The enlarged view of marked region of CI-S6 sample indicates a network of microcracks (Fig. 4). The sizes of these microcracks appear to be slightly larger than that observed with Al₂O₃ coated test samples, possibly due to the large difference in the magnitude of thermal conductivity between the substrate and coated material. The thermal conductivity of ZrO₂5CaO is found between 2 to 4 Wm⁻¹K⁻¹, where as it varies from 33 to 37 Wm⁻¹K⁻¹ for alumina. Since the difference in the magnitude of thermal conductivity between cast iron (50 to 55 Wm⁻¹K⁻¹) substrate and Al₂O₃ coating is less, heat is transferred more or less effectively through the coating system, resulting lower level of thermal stresses which in turn producing smaller size microcracks. On the other hand, the difference in thermal conductivity of alumina and cast iron substrate and ZrO₂5CaO is large, higher level of thermal stresses will be developed resulting larger size microcracks. Further, the splats in the coatings are separated by inter-lamellar pores resulting from rapid solidification of the lamellae and very fine void are being formed due to incomplete inter-splat contact in and around un-melted particles.

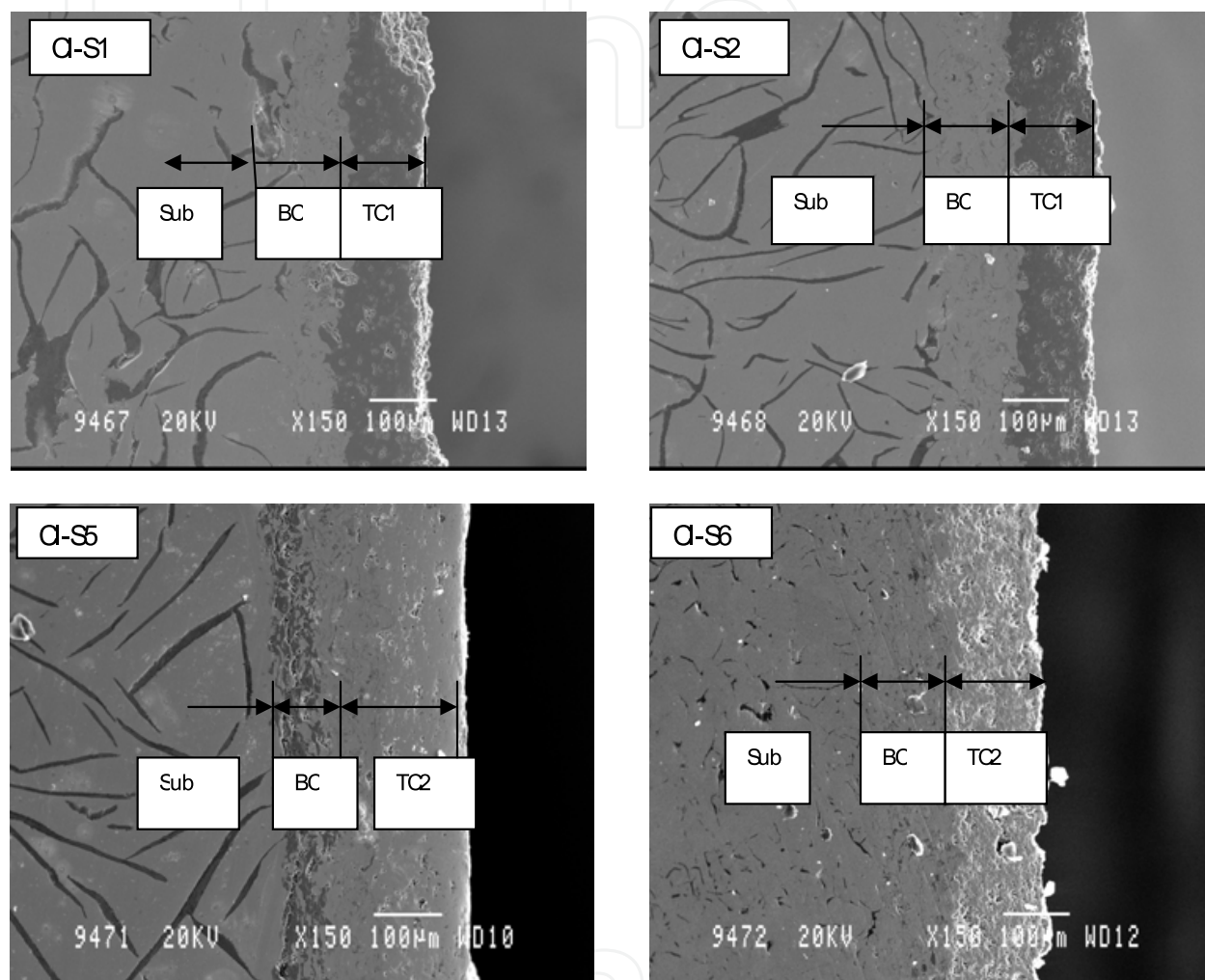


Enlarged View of the Region Marked in CI-S6 Showing Micro-cracks

Fig. 4. Topology of ZrO₂5CaO Coatings on Cast Iron Substrate

3.3 Coating thicknesses and porosity

It is observed that the variation in coating thickness (Fig.5) is about $\pm 25 \mu\text{m}$ from the actual required thickness. This is attributable to the variations in speed of the gun during plasma spraying process. This variation can be minimized by applying Robotic Plasma spraying. Sample polishing technique is also believed to contribute to the variations in the thickness of the coating.



Sub-Substrate BC-Bond Coat (BC1+BC2/ BC3+BC2), TC1-Top Coat 1

Fig. 5. SEM Cross-sections of Al_2O_3 and $\text{ZrO}_2\text{5CaO}$ Coatings

The porosity of Al_2O_3 (CI-S1, CI-S2 and CI-S3) coatings are in the range of 5.7 to 6.4% in case of bond coat and it varies between 6.4 to 7.1% in case of top coat. $\text{ZrO}_2\text{5CaO}$ coated samples such as CI-S4, CI-S5, CI-S6 also shows pores. The porosity of these coatings varies between 6.3 and 6.8% in case of bond coat and 8.2 to 9.4% in case of top coat. Porosity is high, due to formation of rounded pores which are produced by unmelted particles, splats stacking faults and gas entrapment. Porosity of coatings is found to increase with increase in the thickness of top coat.

Porosity formation is due to residual stresses present in coatings. It is found to influence the tendency of the coating to de-bond from the substrate [18-23]. Residual stresses are

introduced into the coatings when the molten particles are quenched upon impact causing a difference in the coefficients of thermal expansion between the coating and the substrate. Residual stresses are also indirectly affected by the pore structure since the stresses depend upon the elastic modulus and magnitude of strain as well. Porosity of $ZrO_2/5CaO$ coatings is slightly higher than that of Al_2O_3 coatings which is due to the larger difference in thermal conductivity between the substrate and top coat in comparison with that found with Al_2O_3 coatings, for the reasons explained earlier.

In the present work, the porosity of coatings is less than that of coating systems reported by Portinha [24].

3.4 X-ray diffraction analysis of coatings

X-ray diffraction (XRD) patterns for the top surfaces of plasma sprayed Al_2O_3 and $ZrO_2/5CaO$ coatings are shown in Fig.6. The XRD patterns of Al_2O_3 coatings show the presence of $\gamma-Al_2O_3$ as a principal phase and $\alpha-Al_2O_3$ as minor phase. It shows that oxidation has occurred during spraying by converting hard phase of Al_2O_3 into soft phase of $\gamma-Al_2O_3$. $ZrO_2/5CaO$ coatings possess tetragonal ZrO_2 as a principal phase and $CaZrO_3$ as minor phase.

XRD patterns suggest that Al_2O_3 particles are not completely transferred into soften $\gamma-Al_2O_3$ phase after the plasma spray process. This is a good result for tribological behavior of coatings where the hardness plays an important role in wear resistance due to abrasion and erosion. The hardness of Al_2O_3 coating is lower than that of bulk alumina (HV-2045) which is mainly due to the intrinsically lower hardness of $\gamma-Al_2O_3$ than $\alpha-Al_2O_3$. The indentation response of a plasma sprayed material is governed not only by the intrinsic hardness of the material, but also by the lamellar microstructure, with splat boundaries giving off under load to facilitate the indenter accommodation [25].

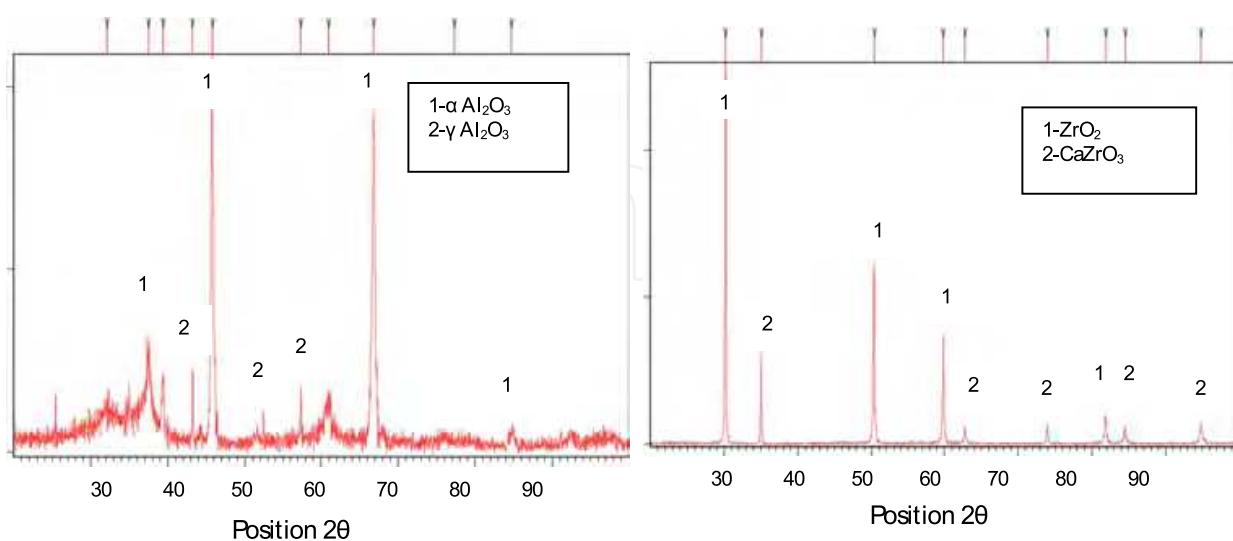


Fig. 6. X-Ray Diffraction Diagrams of Al_2O_3 and (b) $ZrO_2/5CaO$ Coatings

Coating Type	Average Thickness (μm)		Average Porosity (%)			Avg. Surface Roughness (μm)		
	BC	TC1/TC2	BC1	BC2	TC1/TC2	BC1	BC2	TC1/TC2
CI-S1	80	105	5.7	6.2	6.5	4.8	5.8	3.5
CI-S2	100	275	6.1	6.8	6.9	5.3	5.7	5
CI-S3	95	360	6.4	7.0	7.1	5.1	5.5	5.5
CI-S4	100	100	6.3	----	8.2	5.4	----	6.2
CI-S5	85	270	6.5	----	9.0	5.6	----	6.8
CI-S6	85	380	6.4	----	9.4	5.5	----	7.2

Table 4. Thicknesses, Porosity and Average Surface Roughness of Coatings

3.5 Adhesion test – Results

The location of coating failures during the test is described in Table.5.

Samples	CI-S1		CI-S2		CI-S3		CI-S4		CI-S5		CI-S6	
	Strength MPa	Failure Location										
1	20.4	BC3/S	24.8	BC3/S	30.8	BC3/S	37.5	BC3/S	39.8	BC3/S	42.8	BC3/S
2	18.2	BC3/S	20.4	BC3/S	27.4	BC3/S	34.2	BC3/S	34.5	BC3/TC2	46.7	BC3/S
3	22.0	BC3/S	18.8	BC2/TC1	27	BC3/S	32	BC3/TC2	37.6	BC3/S	54	Glue
4	15.8	BC3/S	20.8	BC3/S	29.2	BC3/S	35.4	BC3/S	38.2	BC3/S	45.2	BC3/S
Mean Strength MPa	19.1		21.2		28.7		35.9		38.87		44.2	

BC1/Substrate, BC3/Substrate=Adhesive Failure, BC1/BC2, BC1/TC2, BC2/TC1 and BC3/TC2 = Cohesive Failure, Glue=Failure with in Glue (Poor Test)

Table 5. Adhesion Strength and Failure Location of Coating Systems

The results indicate that the mean values of adhesion for test samples CI-S1to CI-S6. The bond strength is found to increase with the increase in the thickness of the top coat. Analysis of the chemical composition of CI substrate and that of the bond coat layer (BC3) for these samples indicate that the bond coating material consists of as high as 52% of Fe. This will influence the possibility of fusing Fe into the cast iron substrate since the time of exposing the substrate to the plasma spray gun is more in case of samples CI-S2, CI-S3, CI-S5, CI-S6. This probably explains the reason for high adhesion strength of samples coated on cast iron substrate. Fig.7 shows the fracture of samples at substrate/bond coat interface.

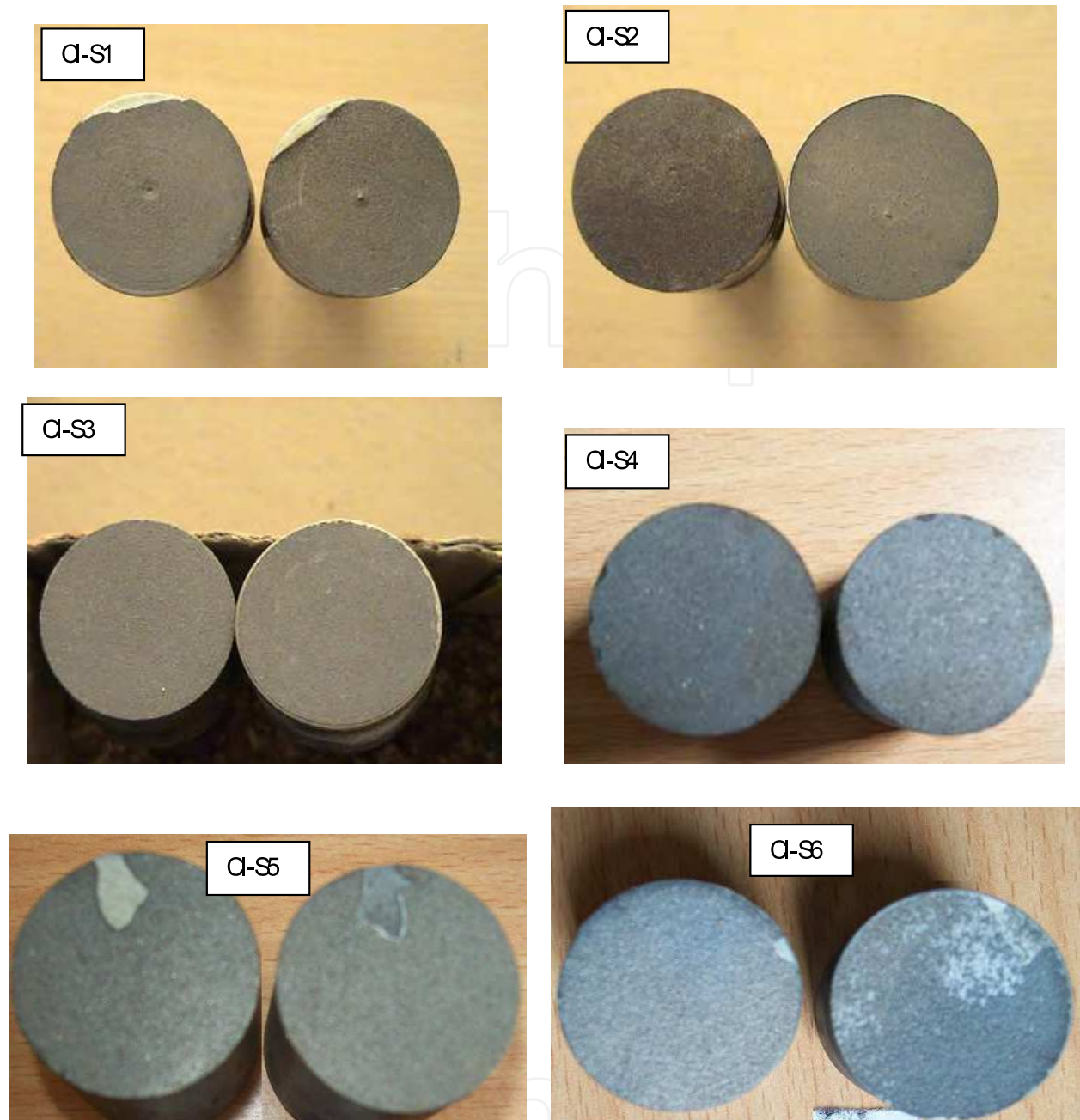


Fig. 7. Fractured Surfaces of Coating Systems after ASTM C633 Tensile Test- Bond Coat/ Substrate Interface

But this simple explanation did not represent the exact behavior of each distinctive coating system. A deep analysis can bring up much more information about the behavior of each individual coating system. It is observed further from Table 5, that the location of the coating failure is at the interface between bond coat and substrate. This is called as adhesion failure. It is seen that in the case of sample 4 of CI-S6, that the failure have occurred at 54 MPa along the glue line. It means that a higher value of adhesion strength could probably found for the above specified samples. Sample 3 of CI-S2, 3 of CI-S4 and 2 of CI-S5 have shown the occurrence of fractures at bond coat/ceramic or bond coat/cermet interfaces respectively. This is attributable to the defects at the bond coat/ceramic interface.

Stress-strain relations (Fig. 8) of the samples show two distinct regions. The first region is due to initial slipping of specimen from the fixtures of UTM. The second region is due to the elongation of specimen at bond coat/substrate interface. Neglecting the strain in first region, the strain percentage in the second region is found to vary between 5 to 6%. It clearly indicates that the specimens in tensile test are ductile in nature.

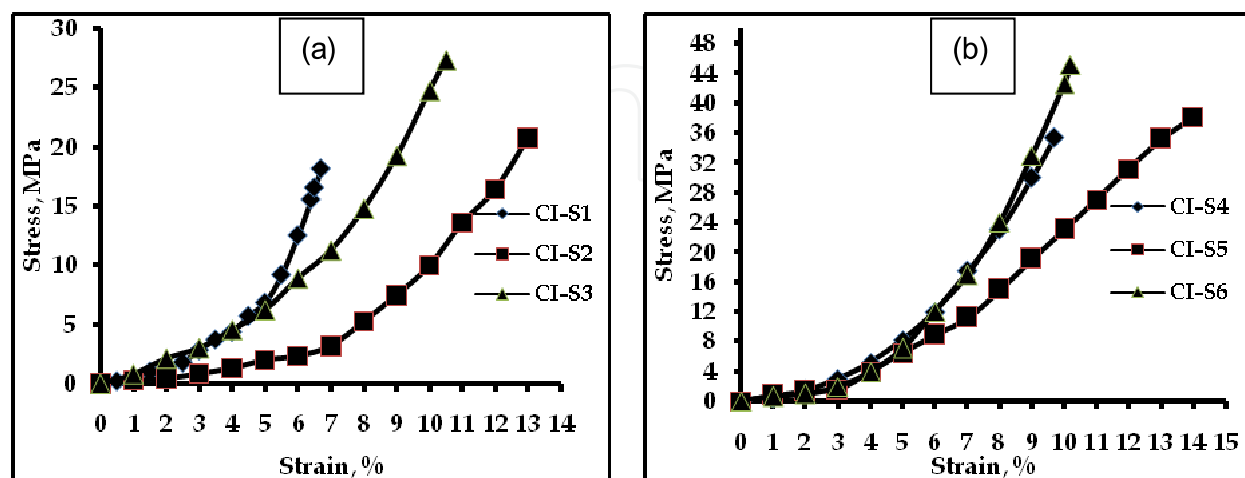


Fig. 8. Stress v/s Strain Diagram for (a) Samples 1, 1, 4 of CI-S1, CI-S2, CI-S3 (b) Samples 3, 3, 4 of CI-S4, CI-S5, CI-S6

3.5.1 Factors affecting adhesion strength of coatings

The amount of adhesion can be evaluated based on degree of coverage [26] of the remaining particles which are bonded after testing of bonding strength. Therefore an adhesion test which presents a singular and partial failure means that true adhesion must be evaluated from that area remaining on substrate after the test which is intact and did not detach or fail. This type of failure can be due to the problems associated with spraying process such as residual stresses, inter splats defects or related to test procedure such as sample alignment or traction speed. It is found that interlocking increases with an increase in the density of coat, the velocity of the impinging droplet and roughness of substrate surface and where as it decreases with the increase in the surface tension at substrate/droplet interface. Rebonding of partially melted particles and stress relaxation from local plastic deformation is found to influence the adhesion strength. On the other, in case of multilayered thermal barrier coatings, adhesion strength mainly depends on the proportion of bond coat, top coat and substrate material. Low bond strength is prevalent when there is a low surface roughness and low mechanical interlocking [27].

Hadad et. al [28] comparing adhesion tests found that interfacial toughness tends to increase with Ra for thin coatings (140 μm) and in their experiments, an opposite trend is seen for thicker coatings (330 μm). Since the crack propagation into a smooth interface is easier than into a rougher one, the interfacial toughness should increase with Ra and then they concluded that the residual stress effect would be dominant for thicker coatings. In the present work, all of the coating systems tested has similar thickness values as reported by Hadad et. al. and they could be considered as thick coatings. The highest roughness value is for CI-S6 (7.2 μm) that also presents one of the highest adhesion mean values (44.2 MPa).

Another issue to be observed is that the roughness just after bond coat application. From Table.4, it is evident that bond coat roughness increases with increasing the thickness. According to Khan et. al. [29] the adhesion of the coating increases with the increase of substrate roughness or bond coat surface roughness up to certain limits (about 5 μm) and then decreases. In case of CI-S2, CI-S3, CI-S5, CI-S6, the adhesion increases with increase in bond coat roughness. With the increase of bond coat roughness there is an increase in interfacial toughness due to high compressive stresses associated with high rough surfaces but further temperature and pressure from the spray process affect the residual stress profile and thus the interfacial toughness of the coatings.

Limarga et al. [27] have carried out investigations on multilayered thermal barrier coatings in which they have obtained adhesion strengths between 5 and 23 MPa depending on the proportion of bond coat, Al_2O_3 and ZrO_2 in the coating systems. In their tests the majority of failures are found to have occurred inside the ceramic layer. They have registered highest values of adhesion strength when the interfacial bond coat/ceramic failure has occurred. According to the authors, the very low bond strength exhibited by some coating systems is due to the low surface roughness of the sprayed ceramics, where as the mechanical interlocking is negligible. Further, they have found that the low surface roughness correspond to the small particle size of materials used in plasma spraying has affected the bond strength. Using the same analogy in the present work and by considering the top ceramic layer only, it can be observed from Table 4 that the highest roughness values are found with CI-S4, CI-S5 and CI-S6 with $\text{ZrO}_2\text{5CaO}$ top coat. These coating systems have highest values of adhesion. The grain size of $\text{ZrO}_2\text{5CaO}$ (-53+11 μm) powder is greater than that of Al_2O_3 (-31+3.9 μm) powder which is used as top coat in case of CI-S1, CI-S2, CI-S3 coating systems. This is partially in confirming with that observed by earlier investigator [29]. That is, higher the adhesion strength, higher would be grain size as well as surface roughness.

Lima and Trevisan [30] while working with graded TBCs have found that not only by increasing the thickness, coating adhesion can be decreased but also by increasing the number of coating layers for the same thickness. They have reported that increasing the number of layers has indicated a greater interruption time for the spraying of the subsequent layer due to the time required for making necessary arrangements. In the present work, the only difference with the tested coating systems is the greater number of passes required to deposit Al_2O_3 on CI-S2, CI-S3 and $\text{ZrO}_2\text{5CaO}$ on CI-S5, CI-S6 systems. 40 to 50 % higher number of passes as employed in this investigation implies that an increased number of ceramic interfaces as well as more homogeneous ceramic coating with thinner intermediate layers. This would ensure that the specimen would fracture only at ceramic interfaces in tensile adhesion strength giving higher magnitudes of cohesion.

3.6 Microhardness of coatings

Hardness of different layers of coating systems is indicated in Table.6 and their graphical representations are shown in Fig.9. It is evident that there is a marked difference in microhardness on different layers of coatings. The substrate average hardness varies from 328 to 355 HV, whereas the hardness of BC1, BC2 and TC1 in case of CI-S1, CI-S2 and CI-S3 samples varies from 140 to 160 HV, 130 to 140 HV and 1110 to 1190 HV respectively. In case of CI-S4, CI-S5, CI-S6 samples, the hardness of BC1 and TC2 varies from 145 to 160 HV and

780 to 820 HV respectively. It is also observed that for the first three series coating systems, the BC1 thickness is about 50 μ m and for the next three coatings it is about 100 μ m. From this data it can be realized that the microhardness of BC1 decreases as its thickness increases. Similarly, the hardness of TC1 and TC2 decreases with the increase in their thicknesses. Further, the hardness of Al₂O₃ coatings is found to be more than that of ZrO₂5CaO coatings. It is also evident that the micro hardness measurements exhibit a wide dispersion. Such dispersion in the microhardness values of the coatings is a typical characteristic of APS ceramic coatings clearly attributable to their microstructural heterogeneity [31].

Samples	Hardness HV _{0.3}			
	Substrate	BC1	BC2	TC1/TC2
CI-S1	355	150	135	1190
CI-S2	340	148	130	1158
CI-S3	330	140	140	1110
CI-S4	330	160	-----	820
CI-S5	342	145	-----	800
CI-S6	328	150	-----	780

Table 6. Hardness of Coating Systems

Hardness of the coating is a measure of the resistance to plastic deformation. It is widely recognized that the hardness increases with the increase in the density, i.e. by decreasing the number of pores and micro-cracks. Therefore the hardness of the top coat is a measure of the amount of sintering and integrity and can provide information about the temperature history of the top coat. Bond coat hardness has no effect on life of TBC.

Microhardness measurements of coatings have specific implications with regard to their basic science and technological applications. The effective hardness of a microvolume of a material depends on the cooling rate, phase structure, crack size and distribution, residual stress and strain of the local environment as well. Thus by examining the variation of microhardness within the coatings ensures avenues to understand the processing, structure and property relationships of coatings. Hardness tests may be related to the tensile adhesion tests since both these measurements rely on deformation under stress. Moreover, microhardness studies can give the variation of strength and the flaw distribution throughout the specimen, whereas the strength tests yield the strength of the weakest link of the system.

Portinha [32] has reported about the decrease in microhardness towards the surface in variable porosity samples and slightly increase in microhardness in case of samples with constant porosity. The decrease in microhardness for the graded samples is attributed to the increase in porosity along the cross section. Samples with constant deposition parameters have exhibited only marginal porosity towards the surface with the increase in the surface temperature during deposition process which also contributes to the enhanced hardness. The variation in microhardness within the given thickness of the coating is due to the variation in local structure which is attributable to the pores or lamellar boundaries. In the present investigation, it is observed that the porosity of Al₂O₃ and ZrO₂5CaO increases with the increase in coating thickness of the samples. From the graphs (Fig. 9) it is seen that the hardness of top coat decreases with the increase of porosity. It shows that the coating systems used in the present investigation are in good agreement with the results reported by Portinha.

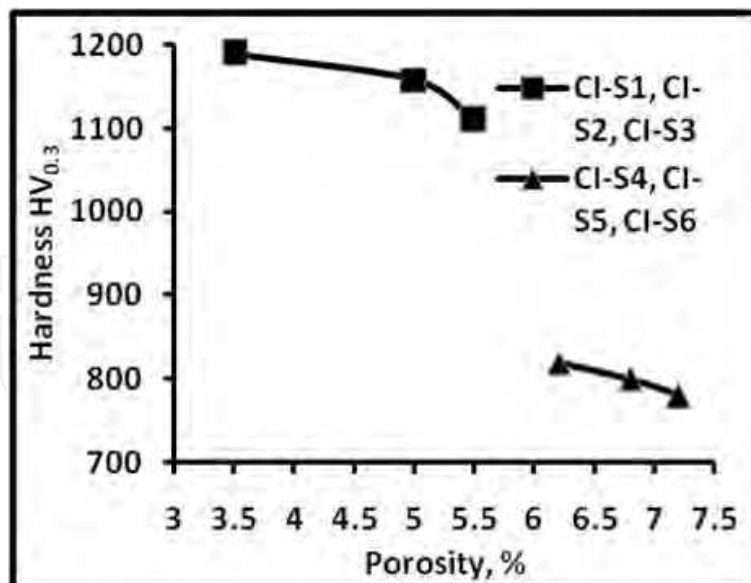


Fig. 9. Variation of hardness with porosity

Microhardness of the coatings increases with the decrease in their porosity. This can be explained based on the principles of microhardness measurements. During the indentation process, a complex elastic-plastic field is formed beneath the indentation. Porosity tends to reduce the effective area supporting the load and is detrimental to strength. When porosity or an equivalent defect is present in a sample, the load bearing area is reduced. It can be safely assumed that the defective region will yield first, thereby inducing strain concentration. However, voids are found to create a multiaxial stress state which can cause local strain concentrations in their vicinity. If all coating systems are considered together, it is obvious that there exists a general tendency that the microhardness decreases with increasing porosity.

3.7 Solid particle erosion test results

3.7.1 Variation of incremental mass loss and cumulative mass loss with time

Fig. 10 shows the photographs of eroded surfaces of coating systems. In erosion test, the samples were allowed to erode by the erodent until a steady state erosion rate was attained. The mass loss of coating systems after every 5 min test is shown in Fig. 11. It is observed that mass loss is suddenly increases in the first 5min of test. After this, mass loss gradually decreases and attains a steady state. From the graphs of cumulative mass loss with time (Fig. 12), it is found that there are two distinct regions under different angles of impact such as 15, 45 and 90° for all coating systems on cast iron substrate. The first region is belongs to erosion of top coat ceramic layer. During this period the slope of erosion mass loss is high and it occurs for a period of 10 to 15 minutes from the starting of the experiment. At normal impact this slope is little higher compared to other angles. The main reason for higher slope during this period is removal of top coat ceramic material. Ceramic layer is made by brittle material which under goes brittle fracture and especially the rate of brittle fracture is high at normal angles of impact. The second region of the graph is occurred due to eroding of cermet and metallic bond layers in case of samples CI-S1, CI-S2 and CI-S3 respectively and only metallic layer in case samples CI-S4, CI-S5 and CI-S6. In this region the slope of erosion mass loss is small compared to that of first region. This region is available till the coating system reaches a steady state erosion condition.

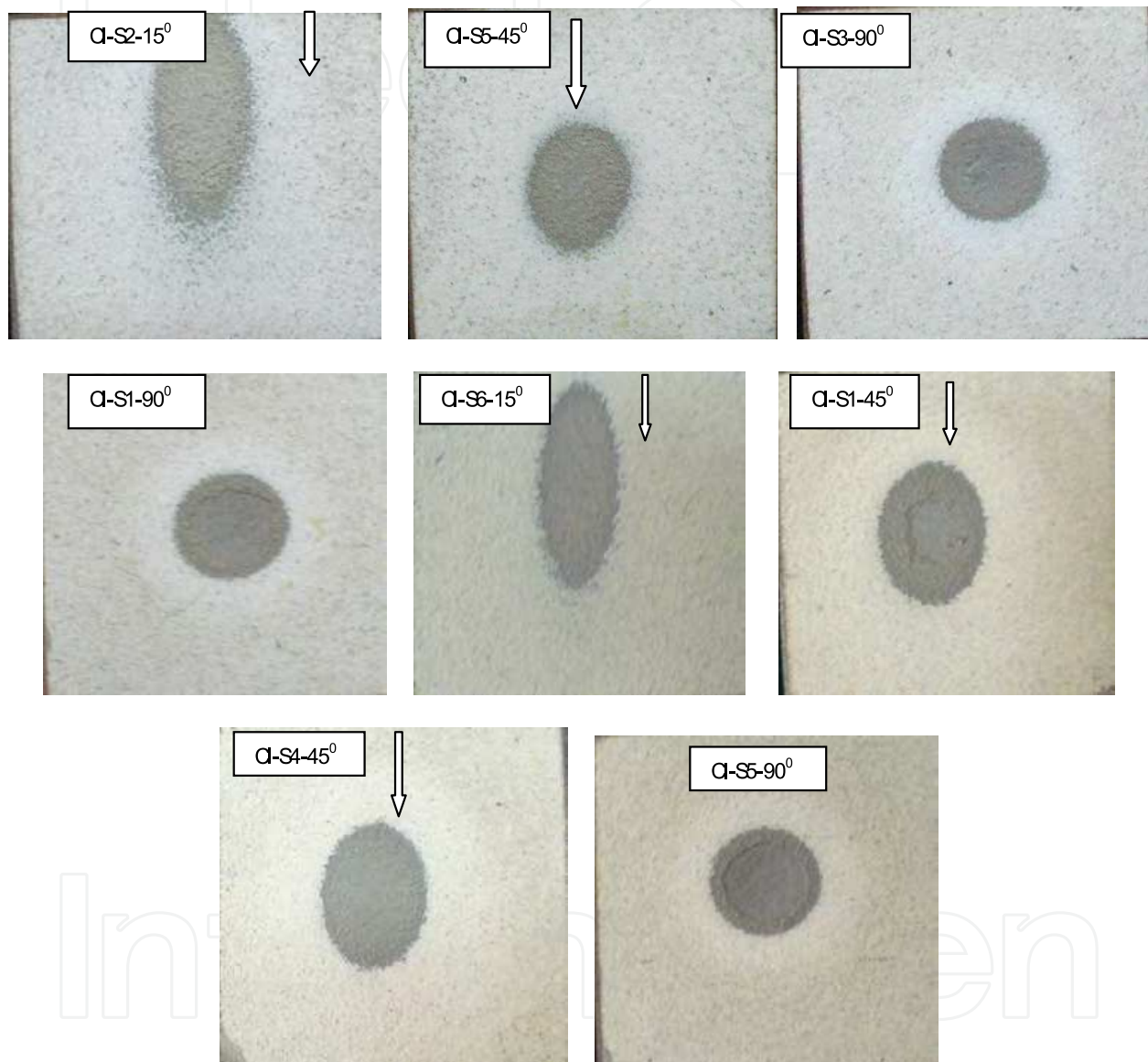


Fig. 10. Photographs of Eroded Surfaces of Al_2O_3 and $\text{ZrO}_2\text{-5CaO}$ Coatings on Cast Iron Substrate 15, 45 and 90 $^\circ$ Angles of Impact (Arrow Mark Indicates the Direction of Silica Sand Jet)

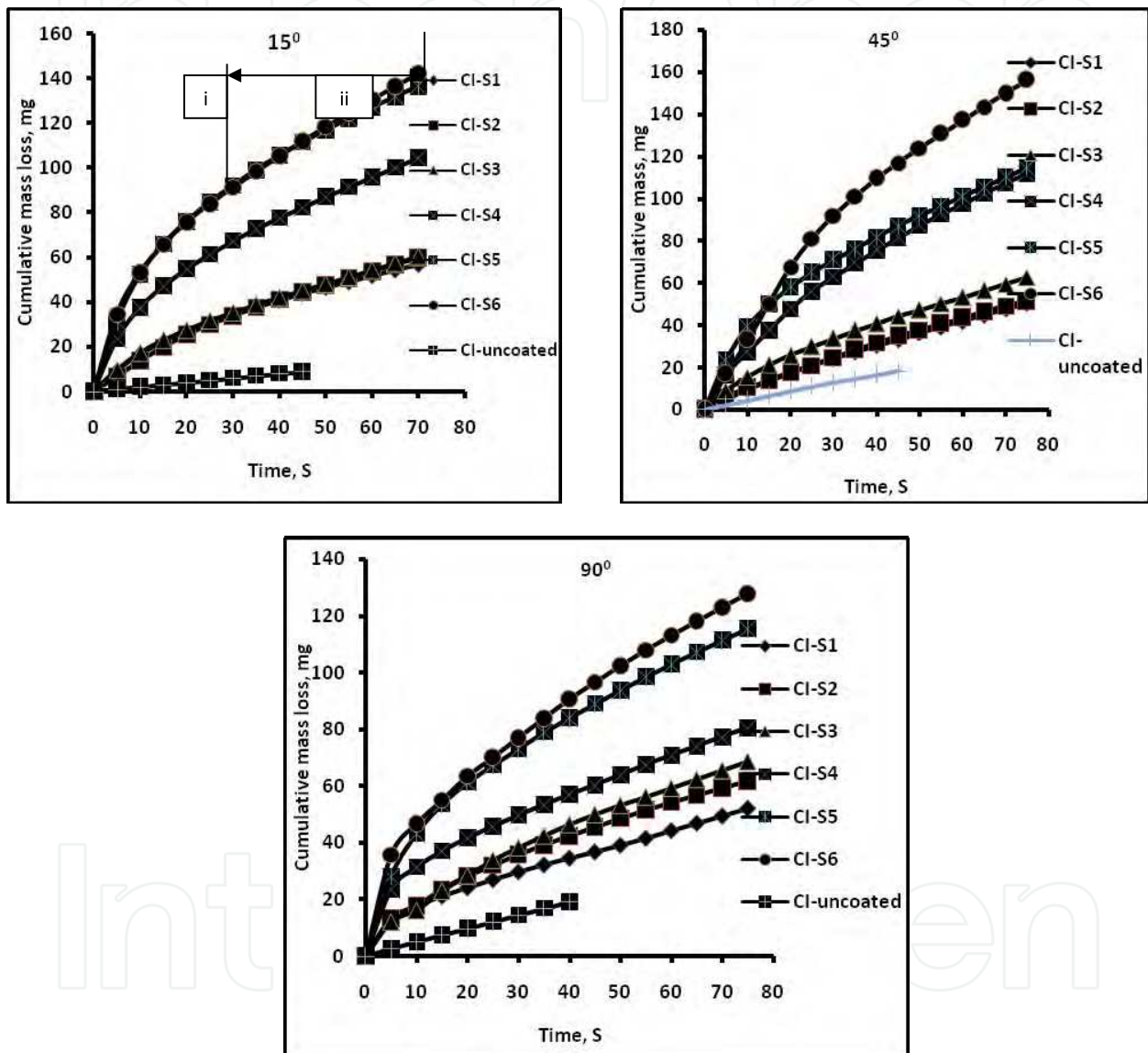


Fig. 11. Cumulative Mass Loss Plots as Function of Time for Alumina and ZrO_2 CaO Coatings on Cast Iron Substrates at 15, 45 and 90° Angle of Impacts

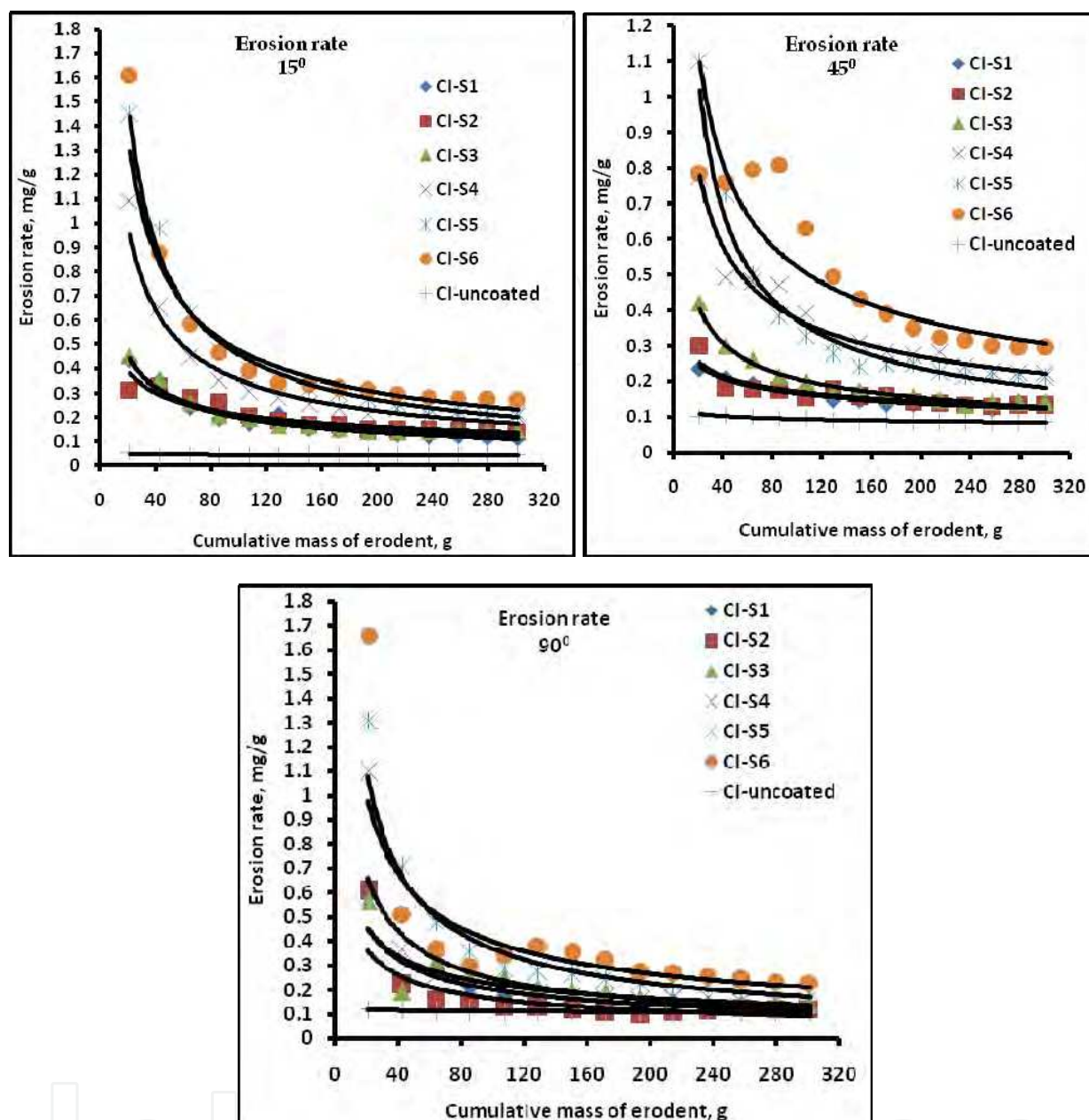


Fig. 12. Erosion Rate Plots as Function of Mass of Eroder for Alumina and ZrO_2 5CaO Coatings at 15, 45 and 90° Angle of Impacts

Cumulative mass loss with time graphs (Fig. 12) shows that the mass loss varies with angle of impinging. According to some engineering model developed so far, for erosive wear, it has been established that the angle at which the stream of solid particles impinges the surface influences the rate at which the material is removed from the surface. This angle determines the relative magnitude of the two velocity components of the impact namely, the component normal to the surface and parallel to the surface. The normal velocity component will determine how long the impact will last and the load. The product of this contact time and the tangential velocity component determine the amount of sliding that takes place. The tangential velocity component also provides a shear loading to the surface, which is in addition to the normal load that the normal velocity component causes. Hence as

this angle changes the amount of sliding that takes place also change as does the nature and magnitude of the stress system. Both of these aspects influence the way a material wears. From the graphs (Fig. 12) it can be realized that the erosion mass loss is more at 45° angle of impinging. In most of the materials, solid particle erosion behaviour can be categorized as being either brittle or ductile in nature [7]. The major differentiating characteristic of the two types of mechanism is the dependence of erosion rate on impact angle i.e. the angle between the moving erodent particle and the material surface [8]. There is a general agreement that maximum erosion occurs at a low angle (about 30°) for ductile material and at 90° for brittle material. In this investigation, coating systems possess multilayer comprising a ceramic top coat and two intermediate metal and cermet bond coats in case of CI-S1, CI-S2 and CI-S3 and only metallic bond coat in case of CI-S4, CI-S5 and CI-S6. Since the erosion loss is more at 45° angle of impact, it can be realized that the coating systems behave neither as purely ductile (where the maximum loss is expected around 15-30°) nor purely brittle (maximum loss is expected at 90°) and has a composite behavior. However, the extent of erosion is found to be strongly dependent on impact angle.

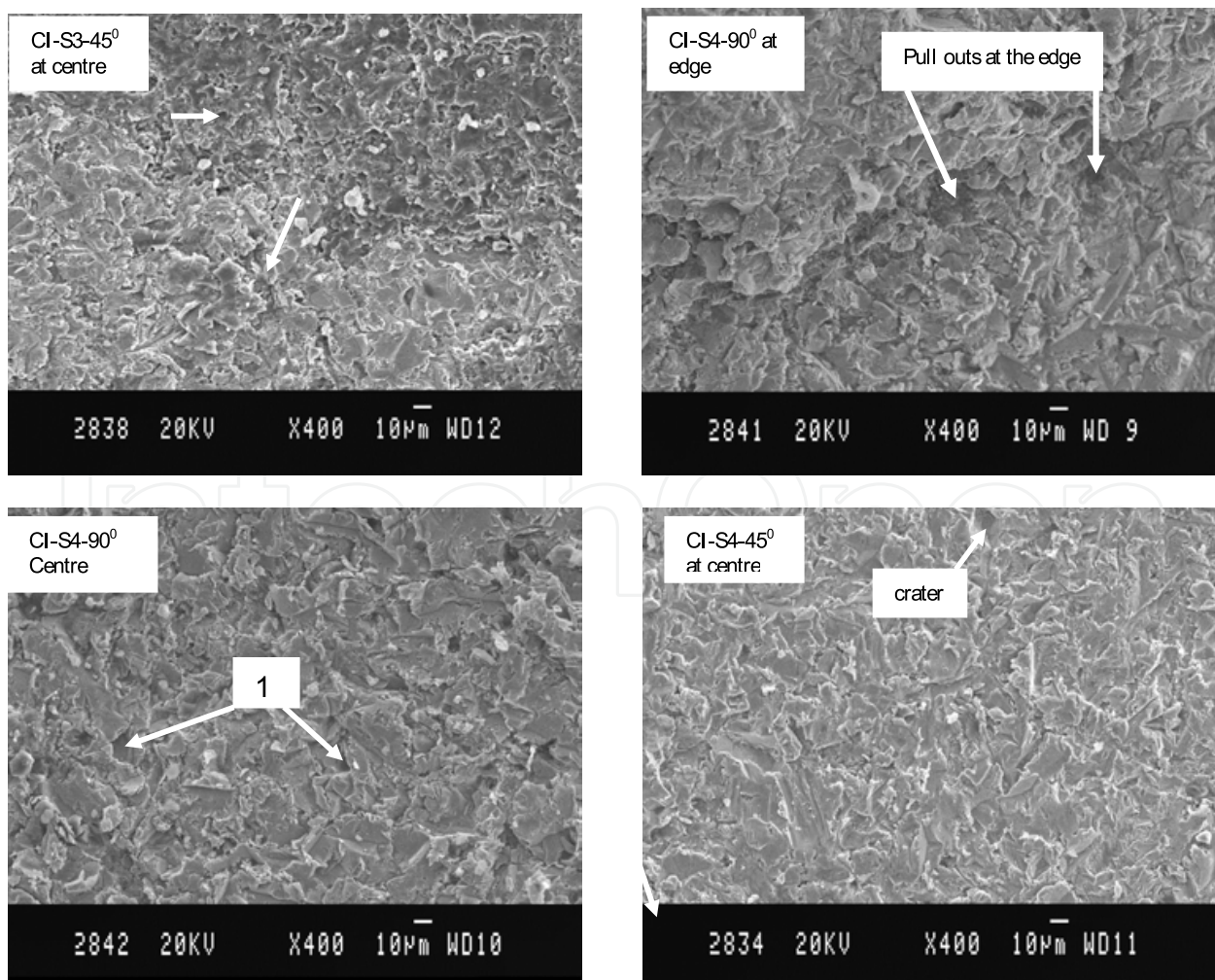
3.7.2 SEM micrographs of eroded surfaces

Fig. 13 shows the surface micrographs of worn out region of the coatings at 15, 45 and 90° impact angles. At lower impact angles (15°, 45°), there are evidences of grooves and ridges (indicated by 1) as the material ahead of the erodent is removed by cutting action. Also material removal may occur from the ridges around the grooves by repeated impacts of erodent. The groove formation may predominantly occur within the softer binder region and this may also result in under cutting of the grains, which may get loosened and eventually pulled out. The pull-out of the grains can also be seen in some regions. At 90° impact angle, indentation impressions due to impingement of erodent on the surface are clearly seen. In ductile erosion one of the common mechanisms is the removal of material from the lips that are formed around the impact craters due to strain localization. The material removal may occur from the displaced material forming lips around the indentations as a result of repeated impacts of erodent. Thus the surface morphology shown in Fig. 13 indicates that the predominant mechanisms are grooving of binder phase, cratering and particle pull-out that are prevalent in the coatings. These mechanisms are responsible for composite erosion mode. The appearance of eroded surfaces also indicates that cracks tend to follow a variety of weak sites to produce wear debris. From the morphology of as-sprayed coatings (Fig. 3 and 4) it is observed that all coating systems possess cracks. Linkage of these pre-existing cracks with indentation cracks could have aided the material removal process. The thermal cracks normal to the surface, the interfaces between adjacent layers of splats can be identified as structural weakness for both Al₂O₃ and ZrO₂5CaO coatings, as described in [33, 34]. The erosion of plasma sprayed coating of lamellar structure occurs through spalling of surface lamella resulting from impact of abrasives. Accordingly the erosion of coating is controlled by the crack propagation along the interface, i.e., the interface bonding between lamellae. Therefore the erosion of the coatings will be dominated by interface bonding condition and lamellar thickness

The eroded surfaces showed evidence of plastic deformation. Ploughing of the surface by the impinging, sharp silica particles, resulting in groove formation, is evident at all angles of

impact, but become more pronounced at lower angles as seen from Fig.13. It is apparent that repeated impacts by the hard particles resulted in highly deformed platelets which are removed by subsequent impacts.

It is well established that in bulk brittle materials such as ceramics, the ratio of particle hardness to the target hardness (H_p/H_t) has a controlling influence in the erosion mechanisms [35, 36]. When this ratio is greater than 1, the wear mechanism essentially involves indentation-induced fracture. At lower ratios cracking is suppressed and the material removal occurs by less severe micro-chipping mechanisms. In the present work, the hardness of erodent (silica) is obtained as 12000 HV. The hardness of Al_2O_3 and ZrO_2 5CaO top coats are 1120-1180 and 830-850 HV respectively. Since H_p/H_t is higher than 1, top coats undergo splat ejection and indentation-induced material removal mechanism. Kingswell et al. [37] have proposed three basic mechanisms of material removal during erosion of thermal spray coatings depending on their microstructure. In poorly bonded thermal sprayed structures, material loss occurs by splat boundary fracture. As splat cohesion is improved, the dominant material removal process becomes splat fracture, micro-chipping and ploughing. Evidently, alumina coatings have a microstructure superior than ZrO_2 5CaO coatings. Due to this alumina coatings have greater resistance to erosion than ZrO_2 5CaO coatings.



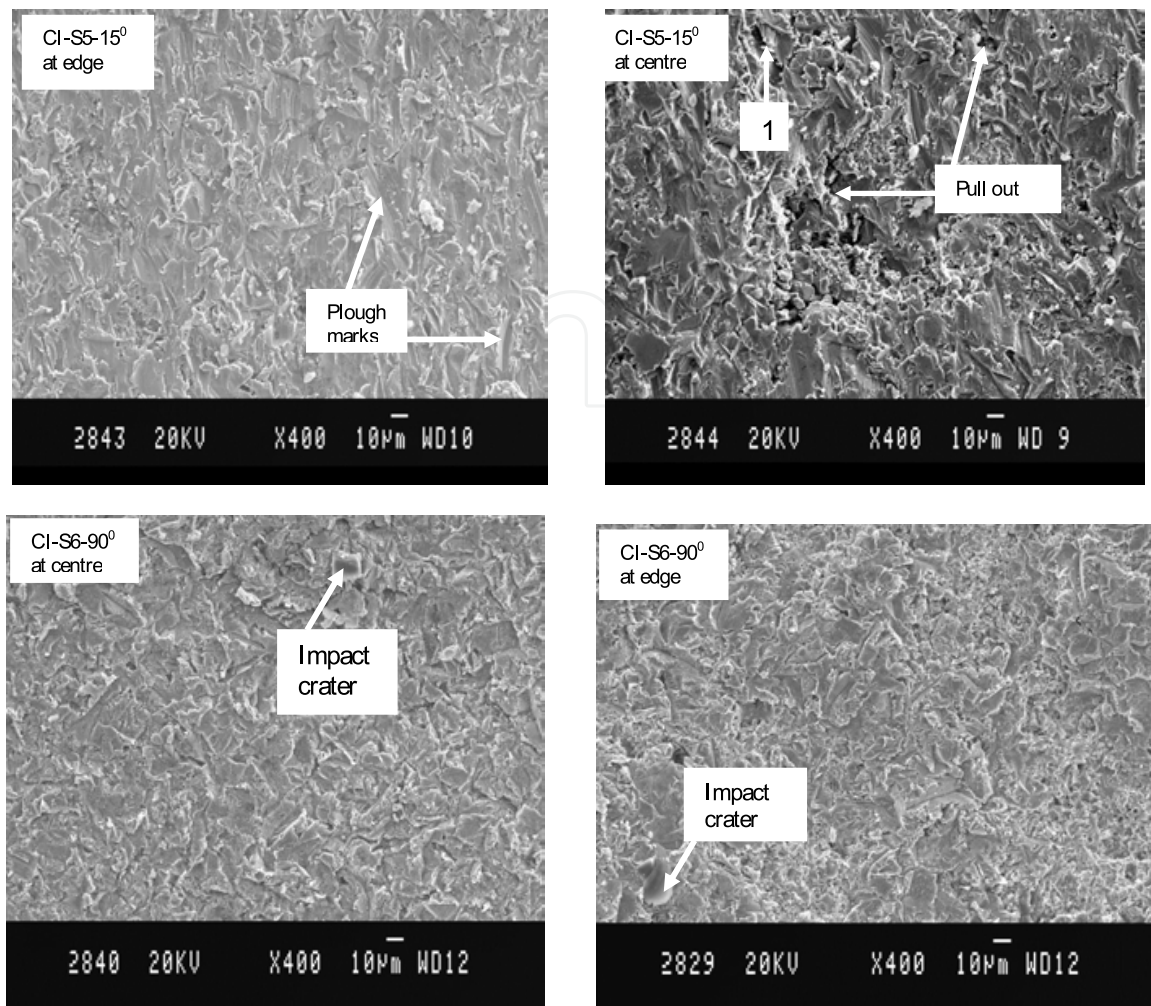


Fig. 13. SEM Micrographs of Eroded Surface of Alumina and $ZrO_2.5CaO$ at Different Angles of Impact.

3.7.3 Incremental erosion rate and volume erosion of coatings

Erosion rate is the ratio of incremental mass loss to mass of erodent per impact (5min. test is considered as one impact). Fig. 14 shows a typical plot of erosion rate as a function of cumulative erodent mass impinging the coating at 15, 45 and 90° impact angles. From the graphs it is found that a transient regime has occurred in the erosion process, during which incremental erosion rates decrease monotonically down to a constant steady state value. The starting period of erosion process is also called as incubation period. The decrease in the erosion rate with erosion time or cumulative erodent mass has been reported before [38]. They postulated that, for some brittle materials, initially the target surface is thoroughly cracked with minimum material loss. Then, significant chipping occurs, which leads to a maximum erosion rate. Further particle impact cracking proceeds, with less material removal.

Later, Levy [38] proposed that incremental erosion rate curves of brittle materials start with a high rate at the first measurable amount of erosion and that it then decrease to a much lower steady state value. Another important factor for high initial erosion rate is high surface

roughness, where protrusions are easily knocked out from as-sprayed surface. Some insight on the reasons for the solid particle erosion transient as observed in this work can come from the current modeling of brittle erosion. According to it, debris is created due to lateral cracking and intersection between various crack types. The size of these cracks varies with load, or equivalently, impact energy. If one starts a solid particle erosion experiment with a target that has a cracking structure with dimensions lower than expected for the impact energy to be used, the incremental erosion rate should increase as the cracking dimensions increase upto a steady state. If, on the other hand, the cracking dimensions and density are higher than what would be imposed by the experiment impact energy, then the erosion rate should start high and decrease to a steady state value, as the cracking dimensions and density decrease. In the case of plasma sprayed coatings, it is possible that the near surface coating has a defect density higher than the bulk coating. With higher crack density the near surface coating toughness decreases and so does hardness, which according to equation $W_E \sim (C_r^2 h) \alpha (1/K^n H^m)$ [39] where W_E , volume loss per impact, C_r , lateral crack size, K and H , coating toughness and hardness, m and n are constants, should determine a higher erosion rate than the bulk coating. Also, since solid particle impact can promote significant surface heating, it is possible that crack closing happens during erosion. The steady state erosion rate is achieved when bond layer of coating systems is exposed to erodent. The steady state erosion is almost same for the systems CI-S1, CI-S2 and CI-S3 but it is different for CI-S4, CI-S5 and CI-S6 and increases with increasing of top coat thickness. The average mass loss of the coatings under steady state erosion rate conditions is taken for comparing the erosion of coatings.

The steady state volume loss of the coatings as a result of erosion at different angles of impact of the erodent is shown in Fig. 14. From this, it is observed that the volume loss is more at 45° angle of impact. The volume erosion loss of cast iron substrate increases with increase of angle of impact showing that the erosion behaviour as brittle. The volume erosion loss of these substrates is less than that of all coating systems. The difference in deformation in uncoated substrates and coating systems can be rationalized based on the deformation response in amorphous and crystalline materials. It is known that amorphous material is prone to shear band formation [40]. Since erosion conditions involve relatively high strain rates, they are quite favorable for shear band formation. The amorphous binder in the plasma sprayed coating systems is expected to form shear bands more easily leading to higher erosion. On the other hand, the deformation in crystalline metal substrates involves strain-hardening leading to higher energy absorption resulting in lower erosion. Cast iron substrate erodes more at 90°. This clearly shows that cast iron follows brittle erosion behaviour. Again, it is found that volume erosion loss of alumina coatings is more than that of ZrO₂5CaO coatings. The volume erosion loss of different coatings at 45° impact is 1.203, 1.23 and 1.12 ×10⁻³cm³ for CI-S1, CI-S2 and CI-S3 (alumina coatings) 0.952, 0.9208 and 0.754 ×10⁻³cm³ for CI-S4, CI-S5 and CI-S6 (ZrO₂5CaO coatings). Although the cumulative mass loss of ZrO₂5CaO coatings is more than that of alumina coatings, the volume erosion loss of these coatings is higher. This is mainly due to higher composite density of ZrO₂5CaO coatings (composite density of ZrO₂5CaO coatings is about 6.3 to 6.96 g cm⁻³ where as density of alumina coatings are about 2.4 to 2.7 g cm⁻³).

3.7.4 Effect of coating hardness on erosion rate

It is well understood that the erosion rates are affected by various factors [4, 41-44]. These factors can be broadly classified into three types: impingement variables describing the

particle flow, particle variables, and material variables. The primary impingement variables are particle velocity, angle of incidence, flux (particle concentration) and target temperature. Particle variables include particle shape, size, hardness, and friability (ease of fracture). Material variables include all the material properties, such as hardness, work hardening behaviour, and microstructure

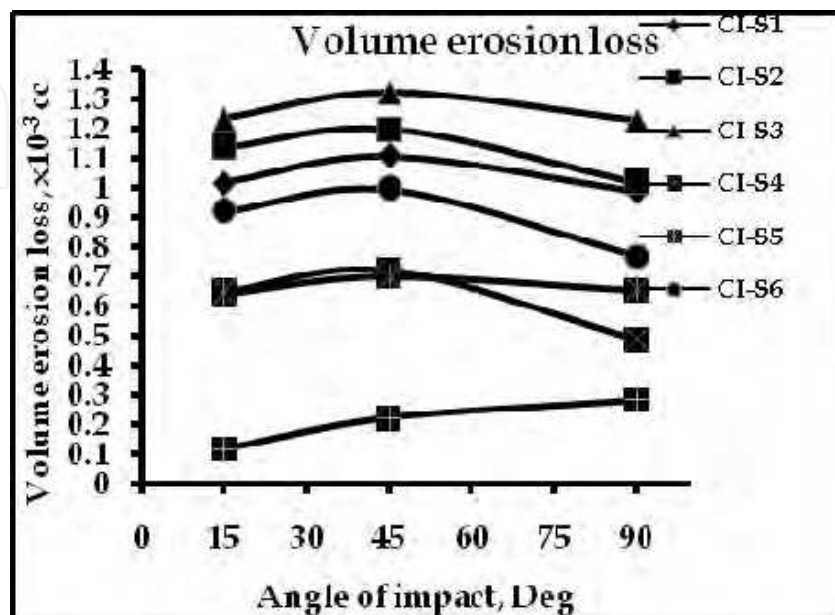


Fig. 14. Volume Erosion Plots as Function of Angle of Impact for Alumina and $ZrO_2/5CaO$ Coatings

Hardness is one of the most effective factors in predicting erosion behaviour and in modeling erosion processes. The best correlation of hardness with erosion is observed for hardness measured on bulk materials [45]. However, few data concerning ceramic coatings are available till now. Here the effect of hardness of coating systems on erosion rate is studied using Vickers hardness. The relationship between erosion rate and hardness of coatings are shown in Fig. 15. It can be seen that a good correlation of hardness with erosion rate is observed irrespective of the type of ceramic. The higher erosion rate is observed at lower hardness of a ceramic coating.

3.7.5 Effect of coating porosity on erosion rate

The erosion rate of plasma sprayed coatings depends on so many parameters like hardness, rupture strength, etc. However, despite the fact that the coatings have very different mechanical properties at the same porosity content, it is the porosity that dictates the erosion behaviour. From the Fig. 16 it is observed that the erosion rate increases with increase of porosity. This result shows that there must be a strong microstructural feature to be incorporated in erosion models. Porosity is definitely one very important feature, which influences erosion in three ways. Firstly, it decreases the materials strength against plastic deformation or chipping, since the material at the edge of a void lacks mechanical support. Secondly, the concave surface inside a void that is not under the shadow of some void edge will see an impinging particle at an angle higher than the average target surface to impact angle. This will be detrimental for brittle materials and beneficial for ductile ones. Finally pores can act as stress concentrators and decrease the load bearing surface.

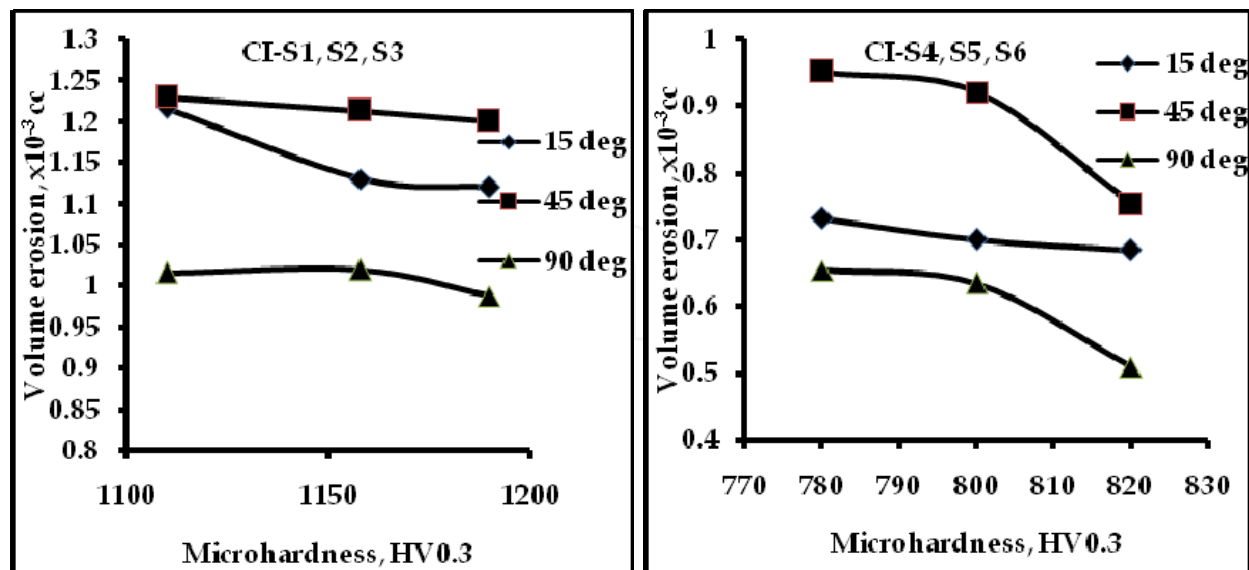


Fig. 15. Effect of Hardness on Volume Erosion of Alumina and ZrO₂.5CaO Coatings

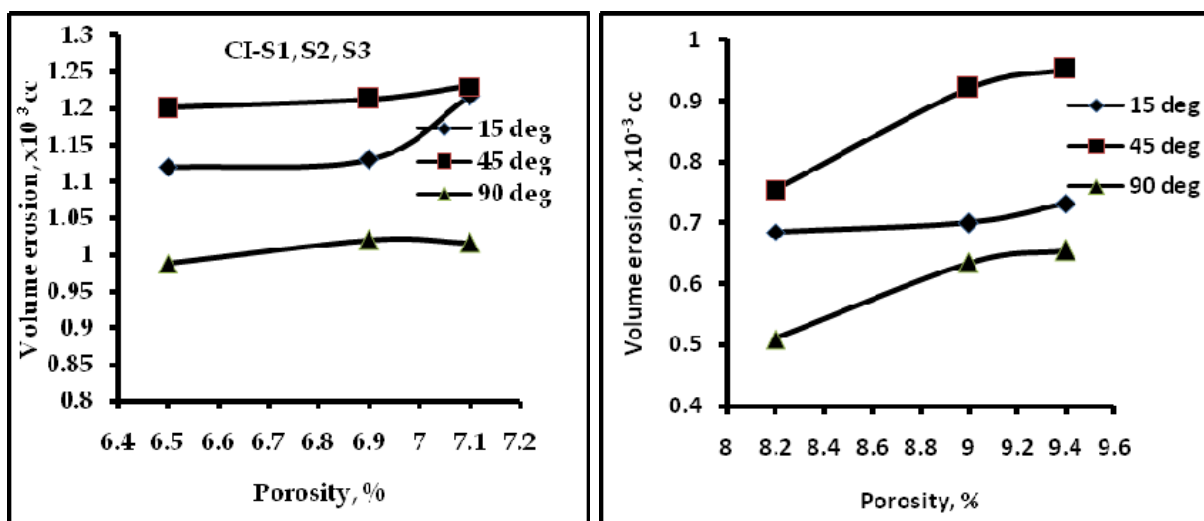


Fig. 16. Effect of Porosity on Volume Erosion of Alumina and ZrO₂.5CaO Coatings

4. Conclusions

- From the study of SEM morphology of the coatings it can be concluded that thermal stresses developed during spraying were main causes for presence of micro-cracks in the coatings.
- From the SEM cross-sections of coating systems it was observed that there is a variation in coating thickness. It is mainly due to variation in speed of the plasma gun during spraying. This variation can be minimized by applying Robot Plasma Spraying technique.
- For adhesion measurement, ASTM C633 tensile adhesion test was used and proved to be effective for general level of comparison. From the obtained results it can be said that the main failure location was in the bond coat/ceramic interface corresponding to the

lowest adhesion values. For the highest adhesion values, coating failure was mainly located in the bond coat/substrate interface. The highest value of adhesion strength was obtained for ZrO_2 5CaO coatings.

- d. By comparing hardness values it can be concluded that Al_2O_3 coating is harder than ZrO_2 5CaO coatings. It can be also concluded that microhardness decreases with increase in coating thickness and porosity.
- e. It was found that erosion of coating systems occurred through spalling of lamella exposed on coating surface resulting from cracking along the lamellar interface. The material removal may occur from the displaced material forming lips around the indentations as a result of repeated impact of erodent. Erosion wear was more at 45° angle of impact showing that erosion behaviour as a composite ductile-brittle. Porosity influences erosion in three ways. Firstly, it decreases the materials strength against plastic deformation or chipping, since the material at the edge of a void lacks mechanical support. Secondly, the concave surface inside a void that is not under the shadow of some void edge will see an impinging particle at an angle higher than the average target surface to impact angle. This will be detrimental for brittle materials and beneficial for ductile ones. Finally pores can act as stress concentrators and decrease the load bearing surface

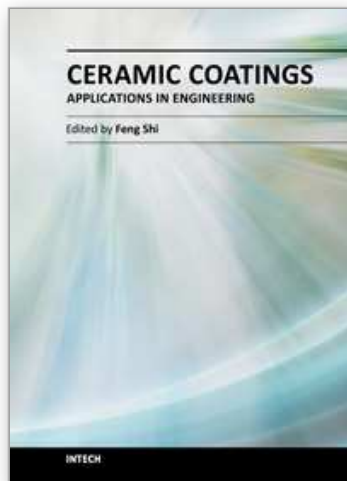
5. References

- [1] Ramesh. C. S, Seshadr. S. K and Iyer, K. J. L, 1991, *A survey of aspects of wear of metals*, Indian Journal of Technology, Vol. 29, pp 179-185.
- [2] Sundararajan. G, *The solid particle erosion of metallic materials: The rationalization of the influence of material variables*, Wear, Vol. 186-187, 1995, pp 129-144.
- [3] Sundararajan. T. and Roy. M. *Solid particle erosion behavior of metallic materials at room and elevated temperatures*, Tribology International, Vol. 30, 1997, pp 339-359.
- [4] Davis. J. R., *Surface engineering for corrosion and wear resistance*, ASM International. 2001.
- [5] Fagoaga, I, Viviente, J. L, Gavin, P, Bronte. J. M, Garcia. J and Tagle. J. A, *Multilayer coatings by continuous detonation System spray technique*, Thin Solid Films, Vol. 317, 1998, pp. 259-265.
- [6] I. M Hutchings, *Tribology: Friction and wear of engineering materials*, Metallurgy and Material Science Series, Edward Arnold Publishing, England 1992.
- [7] G. P. Tilly, Erosion caused by impact of solid particles, *Treatise on materials Science technology*, 13(1979) 287-319.
- [8] I. M. Hutchings, *Recent advances in the understanding of solid particle erosion*, Mecanique Materiaux, 365, 1980, pp 185- 192.
- [9] J. G. Murphy, H. W. King, M. L. Taylor, *Pariculate erosion of zirconia-alumina plasma sprayed coatings I: Ceramic coating erosion mechanism*, The Canadian Ceramic Society, 56, 1987, pp 26-32.
- [10] R. Kingswell, K. T. Scott, S. Bull, *Erosion behaviour of plasma sprayed alumina coatings*, 2nd Plasma Technik Symposium, 1991, Lucerne, Switzerland, pp 367-377.
- [11] X. X. Zhang, I. M. Hutchings, T. W. Clyne, *The effect of deposition conditions on the Erosive Wear resistance of plasma sprayed alumina coatings*, 2nd European Conference on Advanced Materials and Processes, 1991, Euromat 91.
- [12] B. R. Lawn, M. V. Swain, *Microfracture Beneath Point Indentations in Brittle Solids*, J. Mat. Sci., 10, 1975, pp 113-122.

- [13] B. R. Lawn, D. B. Marshall, *Hardness, Toughness and Brittleness: An Indentation Analysis*, J. Am. Ceram. Soc., 62, 1979, pp 347-350.
- [14] B. R. Lawn, R. Wilshaw, Review, *Indentation Fracture: Principles and Applications*, J. Mat. Sci., 10, 1975, pp 1049-1091.
- [15] W.P. Dong, P.J. Sullivan, K.J. Stout, *Comprehensive study of parameters for characterising 3D surface topography II: statistical properties of parameter variation*, Wear 167, 1993, pp 9-21.
- [16] W. P. Dong, P. J. Sullivan, K.J. Stout, *Comprehensive study of parameters for characterising 3D surface topography III: parameters for characterising amplitude and some functional properties & IV: parameters for characterising spatial and hybrid properties*, Wear 178, 1994, pp 29-60.
- [17] O. Sarikaya, *Effect of some parameters on microstructure and hardness of alumina coatings prepared by the air plasma spraying process*, Surf. Coat. & Technol., 190, 2005, pp 388-393.
- [18] P. M. Lonardo, H. Trumpold, L. De Chiffre, *Progress in 3D surface microtopography Characterization*, Ann. CIRP 42, 1996, pp 589-598.
- [19] R. Groppetti, N. Senin, *A contribution to the development of three-dimensional nano and micro-topography measurement and analysis techniques and systems*, in: *Eleventh International Metrology Congress*, Toulon, France, 2003.
- [20] S. Jahamnir, *Friction and Wear of Ceramics*, Dekker, New York, 1994.
- [21] R. Divakar, P. J. Blau, *Wear testing of advanced materials*, ASTM STP 1167, ASTM, 1992.
- [22] T. W. Clyne, C. J. Humphreys, *Improvements in Plasma Sprayed Thermal Barrier Coatings for Use in Advanced Gas Turbines*, Department of Materials Science & Metallurgy, University of Cambridge, Pembroke Street, Cambridge CB2 3QZ.
- [23] Thompson, J. A., Tsui, Y. C., Reed, R. C., Rickerby, D. S. and Clyne, T. W, *Creep of Plasma Sprayed CoNiCrAlY and NiCrAlY Bond Coats and its Effects on Residual Stresses During Thermal Cycling of Thermal Barrier Coating Systems in High Temperature Surface Engineering*, Nicholls, J. and Rickerby, D.S. (ed.), 2000, IoM, Edinburgh, pp 199-212.
- [24] Y. Kubo , Satrou Maezono, Koji Ogura, Toru Iwaio, *Pre-treatment on metal surface of plasma spray with cathode spots of low pressure*, Surf., Coat., Technol., 200, 2005, pp 1168-1172.
- [25] J. Alcala, F. Gaudette, S. Suresh, S. Sampath, *Instrumented spherical micro-indentation of plasma sprayed coatings*, Mater. Sci. Eng. A, 369, 2004, pp 124-137.
- [26] C. R. C. Lima, J. M. Guilemany, *Adhesion improvements of Thermal Barrier Coatings with HVOF thermally sprayed bond coats*, Surf. Coat. & Technol, 201, 2007 pp 4694-4701.
- [27] A. M. Limarga, S. Widjaja, T. H. Yip, Surf. Coat. & Technol. 197, 2005, pp-93.
- [28] M. Hadad, G. Marot, J. Lesage, J. Michler, S. Siegmann, in: E. Lugscheider (Ed.), *Thermal Spray Connects: Explore its Surface Potential*, Proceedings of the International Thermal Spray Conference ITSC, Basel, Switzerland, ASM International/DVS, Dusseldorf, Germany, 2005, pp. 759.
- [29] A. N. Khan, J. Lu, H. Liao, Surf. Coat. & Technol., 168, 2003 pp 291.
- [30] C. R. C. Lima, R. E. Trevisan, J. Therm. Spray Technol. 6(2), 1997, pp 199.
- [31] P. P. Psyllaki, M. Jeandin, D. I. Pantelis, *Microstructure and wear mechanism of thermally sprayed alumina coatings*, Materials Letters, 47, 2000, pp 77-82.

- [32] A. Portinha, V. Teixeira, J. Carneiro, J. Martins, M.F. Costa, R.Vassen, D. Stoever, *Characterization of thermal barrier coatings with a gradient in porosity*, Surf. Coat. Technol., 195, 2005, pp 245-251.
- [33] S. F. Wayne, S. Sampath, *Structure/property relationships in sintered and thermally sprayed WC-Co*, J. Thermal Spray Technol., 1, 1992, pp-307-315.
- [34] H. M. Hawthorne, L. C. Erickson, D. Ross, H. Tai, T. Troczynsky, *The microstructural dependence of wear and indentation behaviour of some plasma sprayed alumina coatings*, Wear 203-204, 1997, pp 271-279.
- [35] J. L. Routbort, R. O. Scattergood, *Erosion of ceramic materials*, Key engineering materials, Vol.71, Trans. Tech. Publications, Switzerland, 1992, pp 23-50.
- [36] S. M. Wierderhorn, B. J. Hockey, J. Mater., Sci. 18, 1983, pp 766-780.
- [37] R. Kingswell, D. S. Rickerby, S. J. Bull, K. T. Scott, Thin solid films 198(1991) pp 139-148
- [38] Levy .A.V, *The erosion-corrosion behaviour of protective coatings*, Surf. Coat. & Technol., 36, 1998, pp 387-406.
- [39] Ives .L. K, Ruff .A. W, Wear 46, 1978, pp 149-162.
- [40] A. L. Greer, K.L. Rutherford, I. M. Hutchings, Int. Mat. Rev. 47(2), 2002, pp 87.
- [41] Kosel, T. H., *Solid particle erosion, in: Friction," in: Lubrication and Wear Technology*, ASM Handbook, Vol. 18, 1992, pp. 199-213.
- [42] Levy. A.V, *Solid Particle Erosion and Erosion-Corrosion of Materials*, ASM International, Materials Park, OH 44073-0002, U.S.A. 1995.
- [43] Sundararajan. G., *The effect of temperature on solid particle erosion,"* Wear, Vol. 98, 1984, pp 141-149.
- [44] Tilly. G. P., *A Two Stage Mechanism of Ductile Erosion*, Wear, Vol. 23, 1973, pp 87-96.
- [45] M. Matsumura, Y. Oka, R. Ebara, T. Odohira, T. Wada, M. Hatano in: W.B.Lisagor, T. W. Crooker, B. N. Leis, ASTM STP, 1049, ASTM Publ., Philadelphia, 1990, pp 521.

IntechOpen



Ceramic Coatings - Applications in Engineering

Edited by Prof. Feng Shi

ISBN 978-953-51-0083-6

Hard cover, 286 pages

Publisher InTech

Published online 24, February, 2012

Published in print edition February, 2012

The main target of this book is to state the latest advancement in ceramic coatings technology in various industrial fields. The book includes topics related to the applications of ceramic coating covers in engineering, including fabrication route (electrophoretic deposition and physical deposition) and applications in turbine parts, internal combustion engine, pigment, foundry, etc.

How to reference

In order to correctly reference this scholarly work, feel free to copy and paste the following:

N. Krishnamurthy, M.S. Murali, B. Venkataraman and P.G. Mukunda (2012). Erosion Behavior of Plasma Sprayed Alumina and Calcia-Stabilized Zirconia Coatings on Cast Iron Substrate, Ceramic Coatings - Applications in Engineering, Prof. Feng Shi (Ed.), ISBN: 978-953-51-0083-6, InTech, Available from: <http://www.intechopen.com/books/ceramic-coatings-applications-in-engineering/erosion-wear-behaviour-of-plasma-sprayed-alumina-and-calcia-stabilized-zirconia-coatings-on-cast-iro>

INTECH
open science | open minds

InTech Europe

University Campus STeP Ri
Slavka Krautzeka 83/A
51000 Rijeka, Croatia
Phone: +385 (51) 770 447
Fax: +385 (51) 686 166
www.intechopen.com

InTech China

Unit 405, Office Block, Hotel Equatorial Shanghai
No.65, Yan An Road (West), Shanghai, 200040, China
中国上海市延安西路65号上海国际贵都大饭店办公楼405单元
Phone: +86-21-62489820
Fax: +86-21-62489821

© 2012 The Author(s). Licensee IntechOpen. This is an open access article distributed under the terms of the [Creative Commons Attribution 3.0 License](#), which permits unrestricted use, distribution, and reproduction in any medium, provided the original work is properly cited.

IntechOpen

IntechOpen